Journal of Materials Chemistry C

PAPER

View Article Online
View Journal | View Issue

Cite this: J. Mater. Chem. C, 2017, 5, 5772

Structural design principles for low hole effective mass s-orbital-based p-type oxides†

Viet-Anh Ha, Francesco Ricci, Gian-Marco Rignanese and Geoffroy Hautier *

Received 1st February 2017,
Accepted 23rd March 2017

DOI: 10.1039/c7tc00528h

rsc.li/materials-c

High mobility p-type transparent conducting oxides (TCOs) are critical to current and future optoelectronic devices such as displays, transparent transistors or solar cells. Typical oxides have flat oxygen-based valence bands leading to high hole effective masses and low mobilities. This makes the discovery of high hole mobility oxides very challenging. Sn^{2+} oxides are known to form Sn-s/O-p mixtures and dispersive valence bands (low hole effective mass). However, not all Sn^{2+} oxides exhibit low hole effective mass, pointing to the importance of structural factors. Here, we analyze the electronic structure and chemical bonding of three Sn^{2+} oxides of interest as p-type oxides: SnO and the two $K_2Sn_2O_3$ polymorphs. We rationalize the differences in their hole effective masses by their Sn–O–Sn angles. As band dispersion is governed by the orbital overlap, Sn–O–Sn angles near 180° maximize the overlap and minimize the hole effective mass. We show that this principle is generalizable to a larger set of Sn^{2+} oxides. Our work leads to simple structural design principles for the development of low hole effective mass oxides based on Sn^{2+} (but also other reduced main group cations) offering a new avenue for the ongoing search for high mobility p-type TCOs.

1 Introduction

Transparent conducting oxides (TCOs) are critical to many technologies, from thin film solar cells to touch screens.[1,2] The commercially available TCOs are *de facto* n-type while their p-type counterparts are lagging behind because of their poor material properties.[2,3] One of the main issues with the currently known p-type TCOs is their lower carrier mobility compared to the best performing n-type oxides. The absence of high mobility p-type TCOs prevents the development of many technologies including transparent electronics.[4] Hence, the discovery, design and development of novel p-type TCOs is a very active field of materials research.[5]

One can chemically rationalize the poor hole mobility of typical oxides by their very flat valence bands with an O-p character which leads to large hole effective masses.[6] The use of certain transition metal cations such as Cu^{1+} can mitigate this problem as their d-orbitals hybridize with the O-p orbitals lowering the hole effective mass.[7–11] However, while the work on Cu-based materials has led to significant progress in the field, p-type TCOs still perform poorly compared to n-type oxides especially in terms of mobility. One should also mention the recent demonstration of high p-type conductivities in highly doped Cr-based oxides (*e.g.*, Cr_2O_3, $LaCrO_3$, $CuCrO_2$).[12–14] However, the transport mechanism in these materials is polaronic, leading to very low mobilities and excluding their use in various applications such as transparent transistors.

An alternative way of inducing curvature in the valence band is to use reduced main group cations with the $(n-1)d^{10}ns^2$ electronic configuration (Sn^{2+}, Pb^{2+}, Bi^{3+}...). Recently, we performed a computationally driven high-throughput search to identify several low hole effective mass p-type TCO candidates. This large-scale study highlighted the potential of s-orbital-based p-type TCOs.[15,16] Quantitatively, the diffuse s orbital of the $(n-1)d^{10}ns^2$ cations overlaps significantly more with the O-p orbitals than the localized d orbitals of the transition metals. This leads to much lower hole effective masses for oxides based on reduced main group cations ($m_h \simeq 0.2m_o$, m_o being the free electron mass) than for traditional Cu-based chemistries ($m_h \simeq 2m_o$). This finding is in line with the experimental interest in s-orbital-based p-type TCOs, more particularly in SnO.[17–19] It has also motivated further computational studies of Sn^{2+} compounds.[20,21] While the presence of reduced main group cations such as Sn^{2+} can lead to very low hole effective masses, our high-throughput search demonstrated that this is not a sufficient requirement. Indeed, a significant fraction of oxides containing reduced main group cations does not exhibit low hole effective masses. Among the 50 known

Institute of Condensed Matter and Nanoscience (IMCN), Université Catholique de Louvain, Chemin étoiles 8, bte L7.03.01, Louvain-la-Neuve 1348, Belgium.
E-mail: geoffroy.hautier@uclouvain.be

† Electronic supplementary information (ESI) available: Computational details, projected band structures and Crystal Orbital Overlap Populations (COOP). See DOI: 10.1039/c7tc00528h

Sn^{2+} oxides present in the Inorganic Crystal Structure Database (ICSD),[22] only a handful of materials ($K_2Sn_2O_3$ and $Rb_2Sn_2O_3$ in different polymorphs) show exceptionally low hole effective masses. This demonstrates that not only the chemistry (*i.e.*, the presence of certain cations) but also the crystalline structure plays an important role in determining the hole effective masses.

In this work, we precisely investigate the structural factors leading to low hole effective masses in $(n-1)d^{10}ns^2$ oxides. We focus on Sn^{2+} oxides and analyze the electronic structure and the character of the valence band for SnO as well as for two $K_2Sn_2O_3$ phases. We rationalize the much lower hole effective mass present in the $K_2Sn_2O_3$ phases in comparison with SnO in terms of their very different Sn–O–Sn angles. Angles close to 180° maximize the overlap between the Sn-s and O-p orbitals and lead to lower hole effective masses. We demonstrate the generality of this simple principle on a larger set of known Sn^{2+} oxides. Our analysis leads to a new design principle for low hole effective mass Sn^{2+}-based p-type oxides requiring Sn–O–Sn angles as close as possible to 180°. These guidelines will be of great help to the development of s-orbital-based high mobility p-type TCOs.

2 Methods

All computations have been performed within the density functional theory (DFT) using the generalized-gradient approximation (GGA) exchange–correlation functional in its Perdew, Burke, and Ernzerhof (PBE) version. We used the VASP package and projector augmented wave (PAW) pseudopotentials.[23,24] The effective mass tensors were computed using the approach outlined in our previous work and using the Boltztrap code.[25] Details of the procedure are available in ref. 15 and 26. The hole effective mass (m_h) is a symmetrical tensorial property:

$$\mathbf{m}_\mathbf{h}^\mathbf{T} = \begin{pmatrix} m_{11} & m_{12} & m_{13} \\ m_{12} & m_{22} & m_{23} \\ m_{13} & m_{23} & m_{33} \end{pmatrix} \quad (1)$$

This symmetrical second-rank tensor has three real eigenvalues and associated principal directions (eigenvectors). In the following, we will report these three eigenvalues in order to compare the different materials.

The creation of the input files and the processing of the output files are performed using the Pymatgen code.[27] The band structures are obtained along high-symmetry lines following the conventions introduced in ref. 28. The Crystal Orbital Overlap Population (COOP) analysis is performed using the Lobster package.[29,30] All the visualizations of the crystal structures and of the charge densities are obtained using VESTA.[31] All the data on effective masses will be available in a future publication.[32] More details can be seen in the ESI.†

3 Results

The most investigated s-orbital-based p-type TCO is currently tin monoxide (SnO). It has been widely studied experimentally[17,18,33] and computationally.[19,34,35] Its tetragonal (*P*4/*nmm*) unit cell is shown in Fig. 1(a). It consists of layers of square out-of-plane coordinated Sn^{2+} sharing O^{2-} vertices.

Fig. 2 shows the DFT band structure of SnO along the high-symmetry lines of the Brillouin zone. Due to its tetragonal symmetry, SnO shows only two hole effective mass eigenvalues: one along the Γ–Z direction of $0.59m_o$ and another of $2.8m_o$ in the plane perpendicular to the former direction (for instance, along the Γ–X direction). These directions correspond respectively to inter-layer and intra-layer transport (Fig. 1(a)). It is remarkable that the low-hole-effective-mass (high mobility) direction is the one perpendicular to the layers. This is in agreement with the higher mobilities measured in *c*-axis oriented SnO samples.[36]

To relate the hole effective mass to the electronic structure of SnO, we analyzed the character of the valence band using atomic projected band structures, the partial charge densities, and the COOP analysis. In Fig. 2(a), the color scheme for the band structure indicates the Sn or O character of the different bands.

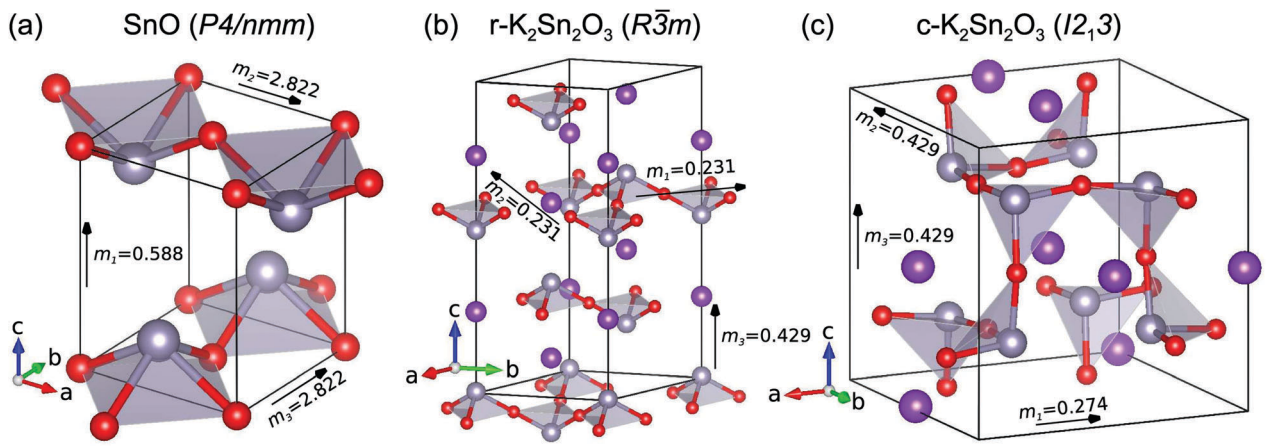

Fig. 1 The conventional cells of (a) SnO with the space group *P*4/*nmm*, (b) r-$K_2Sn_2O_3$, and (c) c-$K_2Sn_2O_3$. The oxygen, tin, and potassium atoms are respectively colored in red, gray and violet. The three principal values of hole effective mass tensor (m_1, m_2, m_3) and their corresponding principal directions are reported in the crystals.

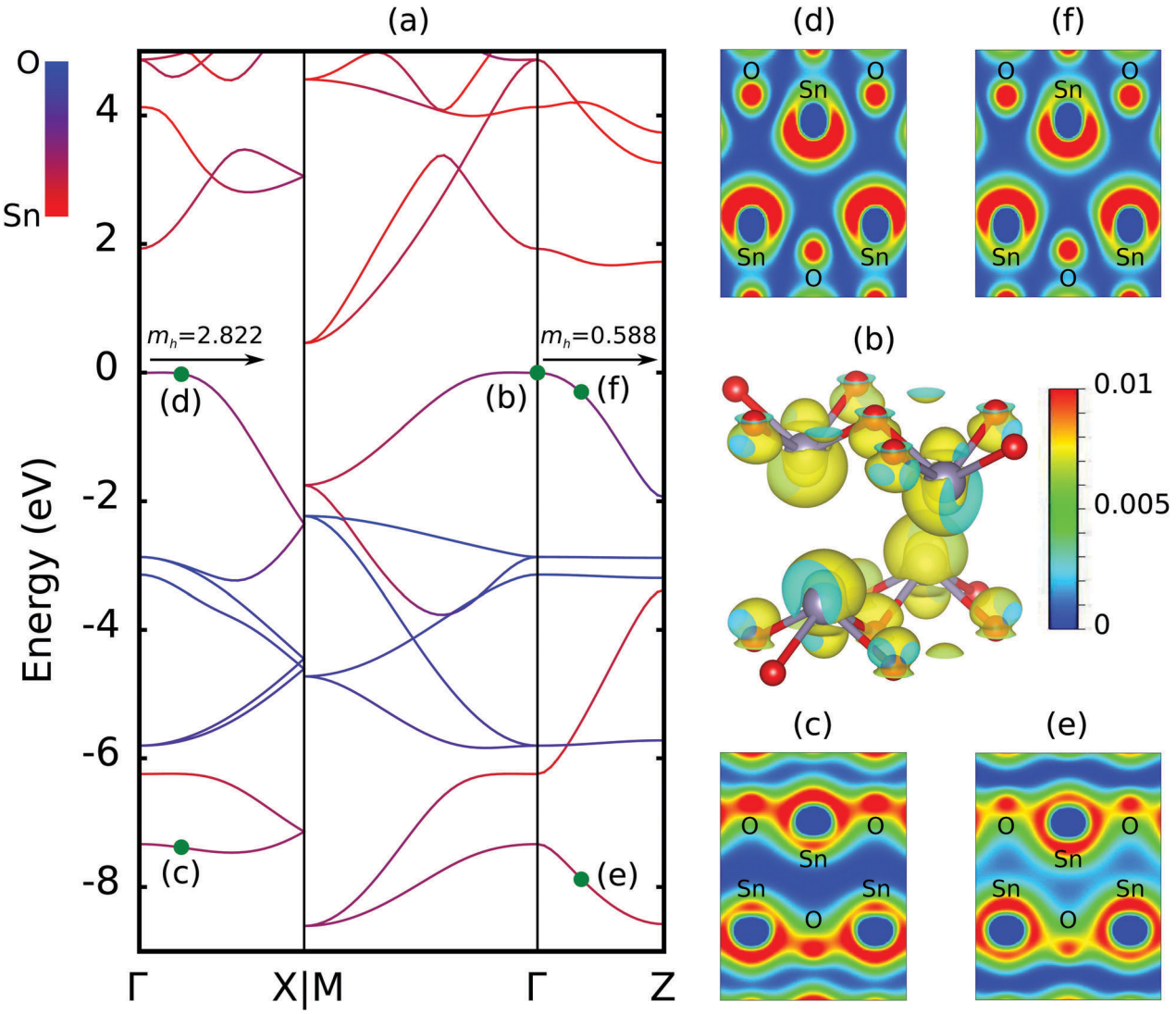

Fig. 2 (a) DFT band structure of SnO, (b) partial charge density at the valence band maximum, and (c)–(f) partial charge density cuts in the (101) plane of the conventional cell (Fig. 1(a)) for two different valence bands at two specific k-points (as indicated in panel (a)). In panel (b), the isosurface corresponds to 0.009 Bohr^{-3}. In panels (c)–(f), the partial charge densities are represented using a color scale ranging from 0 to 0.01 Bohr^{-3}.

The valence band shows Sn and O characters as expected with Sn^{2+} cations. The Sn and O characters of the valence band are also observed in the partial charge density isosurface plot at the valence band maximum (VBM) (Fig. 2(b)). In addition, we carried a COOP analysis (see Fig. S1 of the ESI†). The COOP indicates anti-bonding Sn–O and Sn–Sn characters for the valence band. The linear combination of atomic orbitals (LCAO) theory applied to solids relates the effective mass to the orbital overlap. Larger overlaps lead to lower effective masses.[26,37] Following the previous analysis, the hole effective mass in SnO is driven by the Sn–Sn and Sn–O overlap. Information about the directional dependence of the overlap can be obtained by observing the partial charge densities of the valence band in the two directions. Plane-cuts of the partial charge densities of the valence band (anti-bonding) but also at the corresponding bonding part of the band structure are shown in Fig. 2. Fig. 2(c) and (d) correspond respectively to the plane-cuts for the bonding and anti-bonding partial charge densities in the Γ–X, intra-layer direction. The orbital interaction which is easier to visualize in the bonding state is mainly between Sn and O. On the other hand, Fig. 2(e) and (f) correspond respectively to the plane-cuts for the bonding and anti-bonding partial charge densities in the Γ–Z, inter-layer direction. Here, the bonding state shows weaker Sn–O interaction and a stronger Sn–Sn overlap. The anisotropic transport in SnO is then easily explained by intra-layer orbital interaction due to the Sn–O overlap while inter-layer transport is due to the Sn–Sn orbital interaction.[38]

Among the lowest hole effective mass materials identified by our previous high-throughput study[15] are two Sn^{2+} polymorphs of $K_2Sn_2O_3$: a rhombohedral form (r-$K_2Sn_2O_3$) with space group $R\bar{3}m$ and a cubic one (c-$K_2Sn_2O_3$) with the space group $I2_13$. The synthesis of these two compounds had been reported in the literature but without experimental opto-electronic characterization.[39,40]

The computed hole effective masses of the $K_2Sn_2O_3$ phases are around 0.2 to 0.4m_o and close to the electron effective masses in traditional n-type TCOs (*i.e.*, 0.1 to 0.2m_o).[26] The presence of Sn^{2+} in these oxides is at the origin of its exceptional low hole effective mass as Sn-s orbitals mix with O-p orbitals to lead to a dispersive valence band. However, it has been unclear why the $K_2Sn_2O_3$ phases significantly outperform SnO.

The structure of r-$K_2Sn_2O_3$ in its conventional hexagonal unit cell is reported in Fig. 1(b). Similarly to SnO, r-$K_2Sn_2O_3$ forms a layered structure. Here the Sn–O–Sn network is composed of out-of-plane triangular Sn^{2+} sharing O^{2-} vertices. Fig. 3 shows the DFT band structure of r-$K_2Sn_2O_3$ along high-symmetry lines. Due to the rhombohedral symmetry, the hole effective mass tensor exhibits only two eigenvalues. The eigenvalues corresponding to intra-layer transport (Γ–X direction for instance) are extremely low at 0.23m_o while the inter-layer hole effective mass (Γ–Z direction) is higher but still competitive at 0.43m_o. Similarly to SnO, the atomic projections used for coloring the DFT band structure in Fig. 3(a) indicate the Sn and O mixture at the valence band. Additionally, the Sn and O characters at the valence band are also observed in the partial charge density isosurface plot at the VBM (see Fig. 3(b)). Furthermore, the COOP analysis suggests that the valence band originates from an anti-bonding Sn–O interaction with an important bonding Sn–Sn interaction (see Fig. S2 of the ESI†). The directional dependence of the partial charge densities can also be observed in Fig. 3(c)–(f). The bonding states corresponding to the anti-bonding Sn–O states at the valence band are observed in Fig. 3(c) and (e). The mainly bonding character of Sn–Sn can be observed in Fig. 3(d) and (f). r-$K_2Sn_2O_3$ behaves differently than SnO, which shows a more pronounced difference between the overlap in the intra-layer and inter-layer directions. Nevertheless, the analysis of both oxides leads to the same conclusion that Sn–Sn and Sn–O overlap drives the valence band curvature and the hole effective mass.

In r-$K_2Sn_2O_3$, the intra-layer hole transport is easier than the inter-layer hole transport. The inter-layer transport is similar to

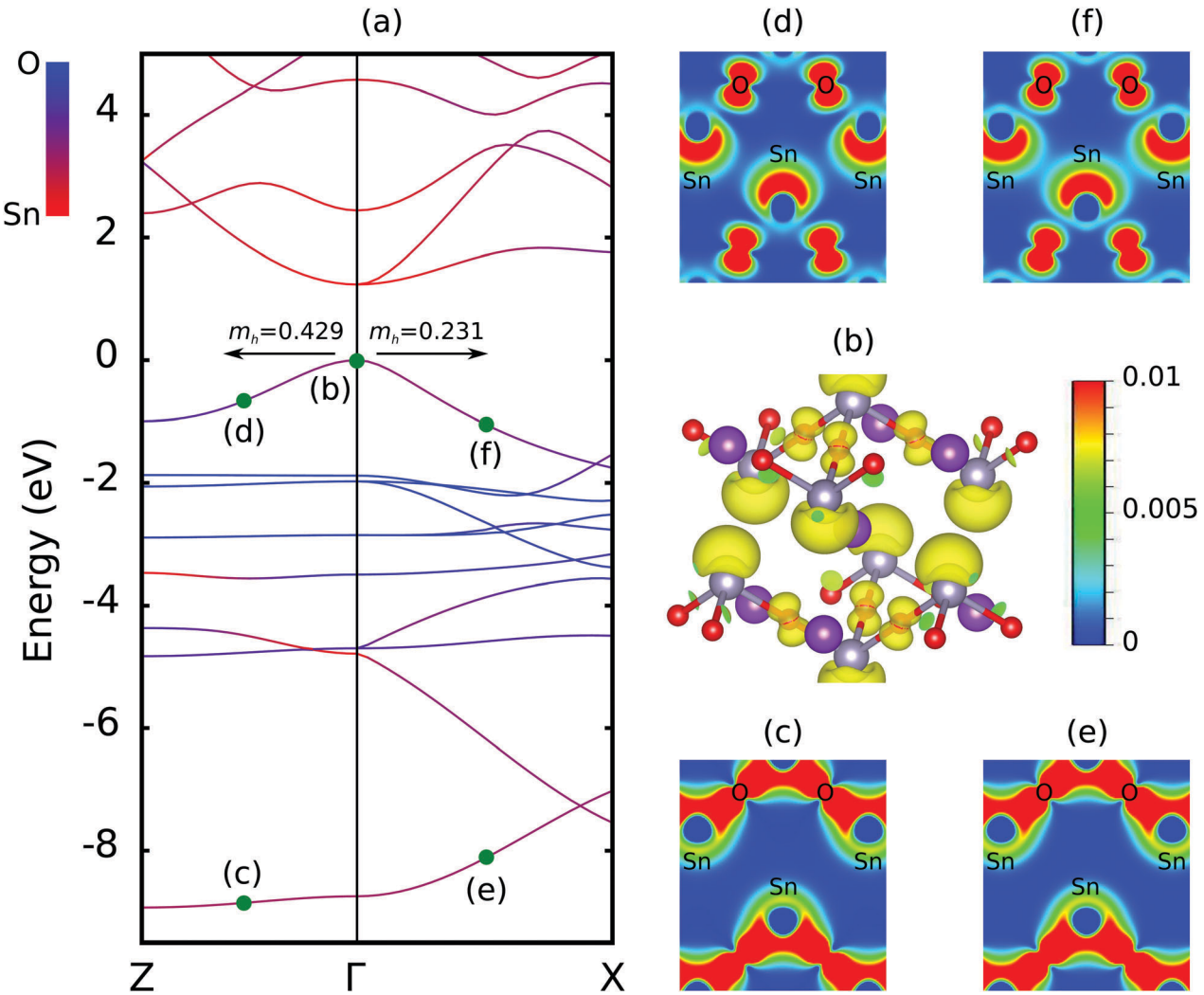

Fig. 3 (a) DFT band structure of r-$K_2Sn_2O_3$, (b) partial charge density at the valence band maximum, and (c)–(f) partial charge density cuts in the $(1\bar{1}2)$ plane of the conventional cell (Fig. 1(b)) for two different valence bands at two specific k-points (as indicated in panel (a)). In panel (b), the isosurface corresponds to 0.012 Bohr^{-3}. In panels (c)–(f), the partial charge densities are represented using a color scale ranging from 0 to 0.01 Bohr^{-3}.

SnO with hole-effective-mass values of 0.43 and $0.59m_o$. On the other hand, the intra-layer hole effective mass is much smaller ($0.23m_o$) than for SnO ($2.82m_o$). The lower effective mass should be the result of stronger orbital overlap between Sn and O. This stronger overlap can naturally be rationalized in terms of the very different Sn–O–Sn angles between r-$K_2Sn_2O_3$ and SnO. In the case of SnO, the Sn–O–Sn angles are around 118° leading to a smaller Sn-s/p to O-p overlap than that of r-$K_2Sn_2O_3$ which shows 180° Sn–O–Sn angles maximizing the s–p overlap. Fig. 4 illustrates how the Sn–O–Sn angle sets the magnitude of the Sn-s/O-p overlap.

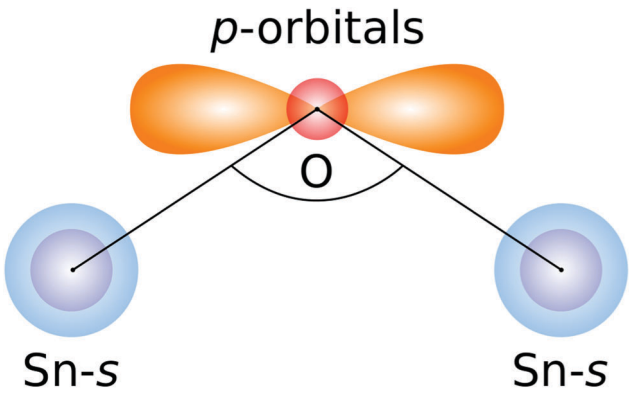

Fig. 4 The angle Sn–O–Sn influences the overlap between Sn-s and O-p orbitals.

The other existing polymorph of $K_2Sn_2O_3$ is cubic (c-$K_2Sn_2O_3$) with the $I2_13$ space group. It also shows extremely low hole effective masses. The crystal structure of c-$K_2Sn_2O_3$ in its conventional cell is reported in Fig. 1(c). Similarly to the rhombohedral phase, the Sn^{2+} cations sit in triangular out-of-plane local environments. These triangular environments share vertices similarly to the rhombohedral phase but do not form a layered structure. Instead, a three-dimensional Sn–O–Sn network is formed. Due to the cubic symmetry, the hole effective mass tensor is isotropic. The unique eigenvalue is very low ($0.27m_o$). The DFT band structure of c-$K_2Sn_2O_3$ is shown in Fig. 5(a) along with the atomic projections. The valence band is also composed of Sn and O characters as visualized in the partial charged density isosurface at the VBM (Fig. 5(b)). In contrast to the layered SnO and r-$K_2Sn_2O_3$, the COOP analysis indicates negligible Sn–Sn overlap and only a Sn–O mixture at the valence band

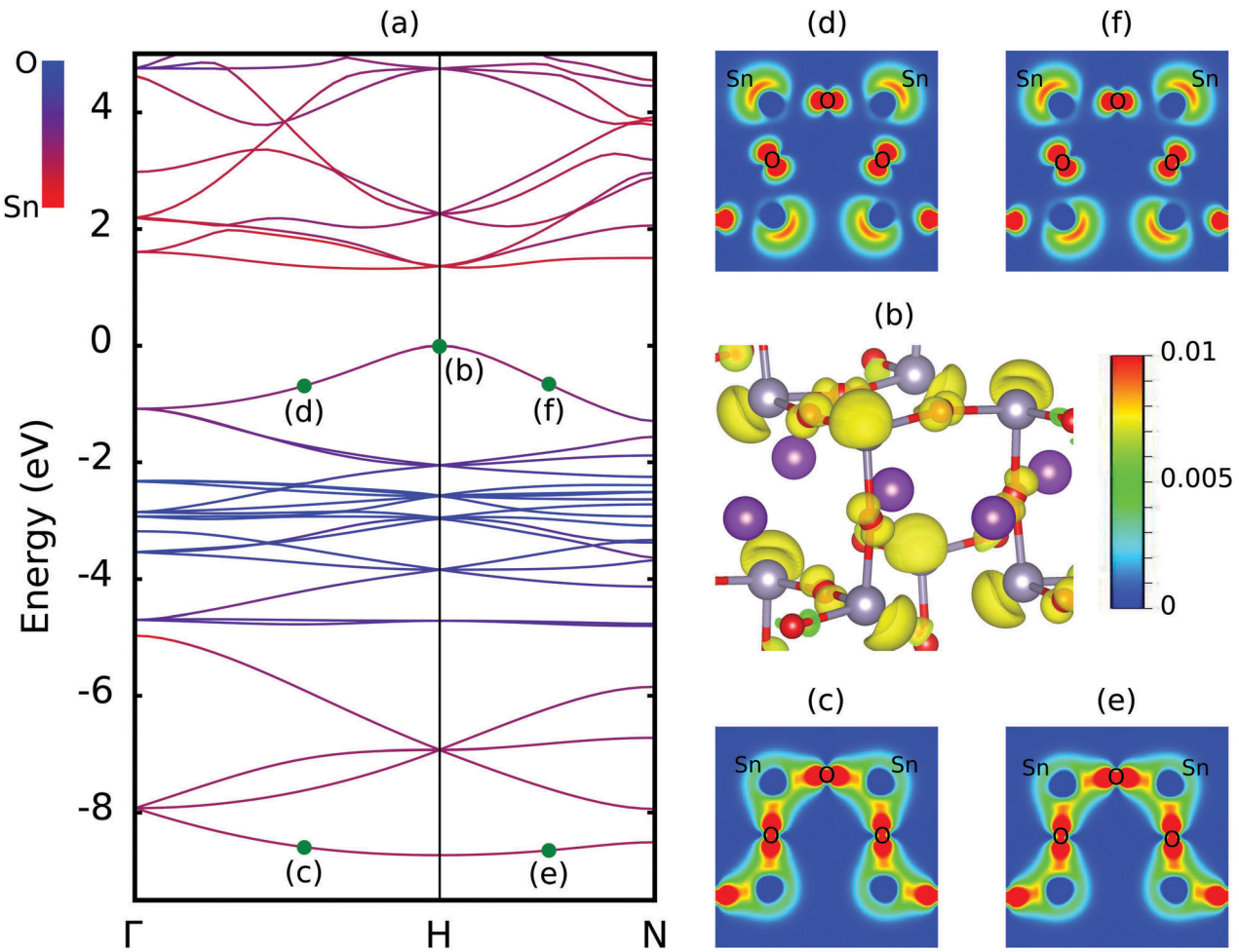

Fig. 5 (a) DFT band structure of c-$K_2Sn_2O_3$, (b) partial charge density at the valence band maximum, and (c)–(f) partial charge density cuts in the (010) plane of the conventional cell (Fig. 1(c)) for two different valence bands at two specific k-points (as indicated in panel (a)). In panel (b), the isosurface corresponds to 0.009 $Bohr^{-3}$. In panels (c)–(f), the partial charge densities are represented using a color scale ranging from 0 to 0.01 $Bohr^{-3}$.

(see Fig. S3 of the ESI†). Plane-cuts of the partial charge densities along two of the crystallographic directions (see pairs of panels (c), (d) and (e), (f) of Fig. 5) at the anti-bonding valence state and the corresponding bonding state clearly shows the Sn–O overlap. Similarly to the intra-layer transport in the rhombohedral phase, the very low hole effective mass emerges here from the large overlap between Sn and O-p orbitals due to the near 180° Sn–O–Sn angle.

Our study on SnO and the two polymorphs of $K_2Sn_2O_3$ shows that the hole effective masses in tin oxide materials are set by Sn–Sn as well as Sn–O overlap. The Sn–O overlap (and therefore the effective masses) will depend strongly on the Sn–O–Sn angle (see Fig. 4). The maximum overlap is obtained when the angle is at 180° and Sn–O–Sn is linear. This rationalizes the much lower effective mass obtained for c-$K_2Sn_2O_3$ and intra-layer r-$K_2Sn_2O_3$, compared to intra-layer SnO. To further test the generality of the importance of the Sn–O–Sn angle in driving Sn^{2+} oxides hole effective mass, we took into account all the available Sn^{2+} oxides present in the ICSD[22] (around 50 compounds). The low number of compounds is indicative of the challenges in the synthesis of Sn^{2+} oxides but also points to the high potential for the discovery of novel Sn^{2+} oxides. As we only focus on the link between effective mass and the Sn–O overlap, we exclude oxides which had an important contribution from other elements than Sn or O at the VBM. We also excluded oxides with isolated Sn–O groups that are not linked together (*e.g.*, $NaSn_4(PO_4)_3$, $Na_2Sn(CO_2)_4$, $SnSO_4$). We notice that none of these excluded oxides presents very low hole effective masses. This leaves us with 18 Sn^{2+} oxides for which we can relate the hole effective mass in a given direction to the average Sn–O–Sn angle. The information on all the ICSD[22] Sn^{2+} oxides is provided in the Tables S1 and S2 of the ESI.† Fig. 6 shows the relationship between the hole effective mass and the average Sn–O–Sn angle of the selected Sn^{2+} oxides. We observe the expected general trend with the lowest hole effective masses being achieved for angles close to 180°. The scattering of the data points can probably be attributed to factors other than the Sn–O–Sn angles such as the Sn–O or Sn–Sn distance and the presence of other species than Sn and O. Sn–O–Sn angles lower than 120° only lead to very large hole effective masses (*e.g.*, $Ta_2Sn_2O_7$). While the lowest hole effective masses are obtained for angles close to 180° in the $K_2Sn_2O_3$ and the isostructural $Rb_2Sn_2O_3$ phases, we notice that angles higher than 120° can lead to already competitive hole effective masses.

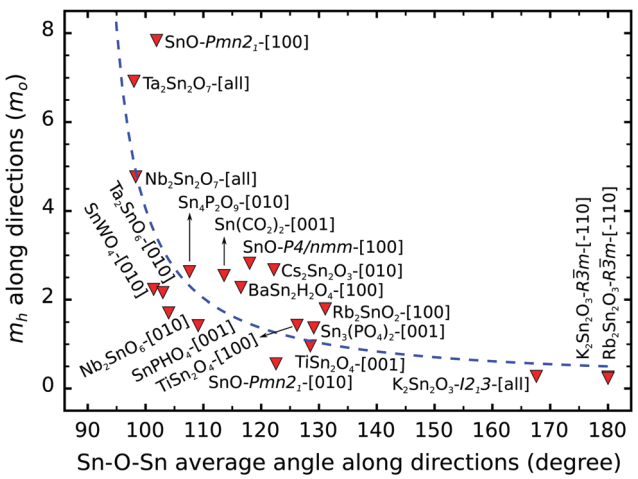

Fig. 6 The hole effective masses (m_h) as a function of the average Sn–O–Sn angle along different directions for various Sn-based oxides. For each data point (red triangles), the chemical formula and the direction are explicitly indicated.

4 Discussions

We have linked the hole effective mass to the chemical bonding in the three Sn^{2+} compounds SnO, r-$K_2Sn_2O_3$ and c-$K_2Sn_2O_3$. Our analysis outlines the importance of the Sn–O–Sn angle in leading to extremely low hole effective masses. Indeed, the Sn–O overlap, which drives the curvature of the valence band in these Sn^{2+} oxides, is maximized for Sn–O–Sn angles close to 180°. Our work leads to simple design principles for achieving low hole effective masses in Sn^{2+} containing oxides. Obviously, the VBM should have only Sn and O-p characters as the presence of other (non $(n-1)d^{10}ns^2$) cations in the VBM character would be detrimental to transport. This is the reason for high hole effective masses in oxides such as $SnMo_5O_8$ or $VSnPO_5$ (see Table S1 of the ESI†). When only Sn^{2+} is present in the valence band, two types of overlap can be observed Sn–Sn and Sn–O. If good hole transport is achieved in all directions (as it is favored for materials used in polycrystalline films), at least one crystalline direction will be influenced by the Sn–O overlap. For this (or these) direction(s), which depend(s) on the Sn–O overlap, the Sn–O–Sn angles should be as close as possible to 180° to maximize the overlap between Sn-s and O-p orbitals.

These design principles explain why many Sn^{2+} compounds do not show low hole effective masses despite the favorable Sn^{2+} chemistry. It also rationalizes why the $K_2Sn_2O_3$ phases are among the lowest hole effective mass oxides reported so far. The potassium atomic levels are low in energy leading to a valence band of Sn and O characters. In addition, the optimal arrangement of the Sn^{2+} out-of-plane triangular environment in the $K_2Sn_2O_3$ phases leads to Sn–O–Sn angles close to 180°. The cubic $K_2Sn_2O_3$ is especially fascinating, as it provides isotropic transport in a fully three-dimensional Sn–O–Sn network with Sn–O–Sn angles close to the optimal value. While we focused here on Sn^{2+} compounds, our design criteria should be extendable to other $(n-1)d^{10}ns^2$ chemistries such as Pb^{2+}, Bi^{3+}, Sb^{3+}…. In fact, the isostructural cubic phase of $K_2Pb_2O_3$ also exhibits a very a low hole effective mass. The best n-type TCOs are based on chemistries related to the reduced main group cations leading to s-orbital-based p-type TCOs. Indeed, compounds containing $(n-1)d^{10}ns^0$ cations such as Sn^{4+} (*e.g.*, SnO_2), In^{3+} (*e.g.*, In_2O_3), Sb^{5+} (*e.g.*, $ZnSb_2O_6$), Zn^{2+} (*e.g.*, ZnO), Ga^{3+} (*e.g.*, Ga_2O_3) show a large overlap with O orbitals as well but in the conduction band.[3] It is therefore natural to wonder if it is also required to have linear metal–oxygen–metal (M–O–M) networks in order to lower the electron effective masses.

The two situations are however slightly different. Previous studies have shown that the conduction band minimum of n-type TCOs shows a significant oxygen-s component.[26,41] No O-s character is present in the valence band of the p-type TCOs based on reduced main group cations and only the strongly directional p orbitals are at play. The O-s character present at the bottom of the conduction band of n-type TCOs should result in electron effective masses less sensitive to the oxygen local environment and to the crystal structure in general. This could explain why cations leading to high performance n-type TCOs in the binaries lead to low electron effective mass oxides even in alternate polymorphs or in ternaries. This is also in line with the common explanation of the good mobility in n-type amorphous TCOs based on non-directional metal oxygen orbital interactions.[42] Interestingly, our finding hints at larger difficulties in making s-orbital-based high mobility p-type amorphous oxides. However, recent studies have shown that percolating lone-pair Sn–Sn interactions could be sufficient to provide good electronic transport in Sn^{2+} amorphous TCOs in three dimensions.[43] Further investigation of the relatively less explored field of p-type amorphous s-orbital-based TCOs could clarify this discussion.

We would also like to point out that it is challenging to find the appropriate crystal structures following our design principle based on the reduced main group cations. Three dimensional linear M–O–M chains are easily formed using centrosymmetric coordination environments (octahedron and tetrahedron). For instance, this is the case in perovskites ABO_3.[44] However, reduced main group cations such as Sn^{2+}, Pb^{2+} and Bi^{3+} are lone-pair active and tend to form non-centrosymmetric environments.[45] For instance, Sn^{2+}-based oxides mainly show square out-of-plane, triangular out-of-plane and see-saw coordination environments.[46] The combination of such distorted environments in order to form three-dimensional networks with linearly coordinated oxygen is possible as demonstrated with the $K_2Sn_2O_3$ phases. It is, however, achieved in relatively rare crystal structures.

Finally, while our work focuses on hole effective mass which is a key property of p-type TCOs, we need to emphasize the multi-property nature of the materials design process in TCOs. In addition to the carrier mobility, which is driven by effective mass, p-type dopability and transparency would need to be taken into account when developing novel p-type TCOs.

5 Conclusions

Very low hole effective masses can be achieved in oxides containing reduced main group cations (Sn^{2+}, Bi^{3+}, Pb^{2+},...). However, the presence of main group cations does not guarantee alone a low hole effective mass. It is thus important to identify the structural factors that influence the hole effective masses. We addressed this question using Sn^{2+} as a typical reduced main group cation. By performing an extensive analysis of the bonding and the electronic structure for three Sn^{2+} oxides proposed as p-type TCOs (SnO, r-$K_2Sn_2O_3$, and c-$K_2Sn_2O_3$), we have identified the Sn–O–Sn angle to be an essential structural factor governing the hole effective masses in Sn^{2+} oxides. Indeed, the Sn–O overlap which drives the curvature of the valence band in these oxides is maximized for Sn–O–Sn angles close to 180°. Not only can the important hole effective mass differences between SnO and $K_2Sn_2O_3$ be rationalized in terms of the Sn–O–Sn bond angle, but the relation between this angle and the hole effective mass also holds for other Sn^{2+} oxides. Our work leads to a series of design principles for low hole effective mass s-orbital-based oxides. In addition to the presence of a reduced main group cation controlling the character of the valence band, a network of metal–oxygen bonds with angles as large as possible (ideally close to 180°) is necessary. We hope that these new design principles will facilitate and motivate future experimental and computational search for novel s-orbital-based p-type TCOs.

Acknowledgements

The authors thank Aron Walsh for helpful discussions. V.-A. H. was funded through a grant from the FRIA. G.-M. R. is grateful to the F. R. S.-FNRS for financial support. GH, GMR and FR acknowledge the F. R. S.-FNRS project HTBaSE (contract no. PDR-T.1071.15) for financial support. The authors acknowledge access to various computational resources: the Tier-1 supercomputer of the Fédération Wallonie-Bruxelles funded by the Walloon Region (grant agreement no. 1117545), and all the facitilies provided by the Université catholique de Louvain (CISM/UCL) and by the Consortium des Équipements de Calcul Intensif en Fédération Wallonie Bruxelles (CÉCI).

References

1 H. Ohta and H. Hosono, *Mater. Today*, 2004, **7**, 42.
2 K. Ellmer, *Nat. Photonics*, 2012, **6**, 809.
3 S. C. Dixon, D. O. Scanlon, C. J. Carmalt and I. P. Parkin, *J. Mater. Chem. C*, 2016, **4**, 6946.
4 E. Fortunato, P. Barquinha and R. Martins, *Adv. Mater.*, 2012, **24**, 2945.
5 K. H. L. Zhang, K. Xi, M. G. Blamire and R. G. Egdell, *J. Phys.: Condens. Matter*, 2016, **28**, 383002.
6 J. B. Varley, A. Miglio, V.-A. Ha, M. J. van Setten, G.-M. Rignanese and G. Hautier, *Chem. Mater.*, 2017, **29**, 2568.
7 H. Kawazoe, M. Yasukawa, H. Hyodo, M. Kurita, H. Yanagi and H. Hosono, *Nature*, 1997, **389**, 939.
8 A. Kudo, H. Yanagi, H. Hosono and H. Kawazoe, *Appl. Phys. Lett.*, 1998, **73**, 220.
9 H. Ohta, M. Orita and M. Hirano, *J. Appl. Phys.*, 2002, **91**, 3074.
10 H. Yanagi, T. Hase, S. Ibuki, K. Ueda and H. Hosono, *Appl. Phys. Lett.*, 2001, **78**, 1583.
11 C. W. Teplin, T. Kaydanova, D. L. Young, J. D. Perkins and D. S. Ginley, *Appl. Phys. Lett.*, 2004, **85**, 3789.
12 K. H. L. Zhang, Y. Du, A. Papadogianni, O. Bierwagen, S. Sallis, L. F. J. Piper, M. E. Bowden, V. Shutthanandan, P. V. Sushko and S. A. Chambers, *Adv. Mater.*, 2015, **27**, 5191.

13 E. Arca, K. Fleischer and I. V. Shvets, *Appl. Phys. Lett.*, 2011, **99**, 111910.
14 L. Farrell, E. Norton, C. M. Smith, D. Caffrey, I. V. Shvets and K. Fleischer, *J. Mater. Chem. C*, 2016, **4**, 126.
15 G. Hautier, A. Miglio, G. Ceder, G.-M. Rignanese and X. Gonze, *Nat. Commun.*, 2013, **4**, 2292.
16 A. Bhatia, G. Hautier, T. Nilgianskul, A. Miglio, J. Sun, H. J. Kim, K. H. Kim, S. Chen, G.-M. Rignanese, X. Gonze and J. Suntivich, *Chem. Mater.*, 2016, **28**, 30.
17 Y. Ogo, H. Hiramatsu, K. Nomura, H. Yanagi, T. Kamiya, M. Hirano and H. Hosono, *Appl. Phys. Lett.*, 2008, **93**, 032113.
18 H. Yabuta, N. Kaji, R. Hayashi, H. Kumomi, K. Nomura, T. Kamiya, M. Hirano and H. Hosono, *Appl. Phys. Lett.*, 2010, **97**, 072111.
19 N. F. Quackenbush, J. P. Allen, D. O. Scanlon, S. Sallis, J. A. Hewlett, A. S. Nandur, B. Chen, K. E. Smith, C. Weiland, D. A. Fischer, J. C. Woicik, B. E. White, G. W. Watson and L. F. J. Piper, *Chem. Mater.*, 2013, **25**, 3114.
20 Y. Li, D. J. Singh, M.-H. Du, Q. Xu, L. Zhang, W. Zheng and Y. Ma, *J. Mater. Chem. C*, 2016, **4**, 4592.
21 Q. Xu, Y. Li, L. Zhang, W. Zheng, D. J. Singh and Y. Ma, *Chem. Mater.*, 2017, **29**, 2459.
22 *Inorganic Crystal Structure Database, 2013*, FIZ Karlsruhe: Karlsruhe, Germany, 2013, https://www.fiz-karlsruhe.de/de/leistungen/kristallographie/icsd.html.
23 G. Kresse and J. Furthmüller, *Comput. Mater. Sci.*, 1996, **6**, 15.
24 G. Kresse and J. Furthmüller, *Phys. Rev. B: Condens. Matter Mater. Phys.*, 1996, **54**, 11169.
25 G. K. H. Madsen and D. J. Singh, *Comput. Phys. Commun.*, 2006, **175**, 67.
26 G. Hautier, A. Miglio, D. Waroquiers, G.-M. Rignanese and X. Gonze, *Chem. Mater.*, 2014, **26**, 5447.
27 S. P. Ong, W. D. Richards, A. Jain, G. Hautier and M. Kocher, *et al.*, *Comput. Mater. Sci.*, 2013, **68**, 314.
28 W. Setyawan and S. Curtarolo, *Comput. Mater. Sci.*, 2010, **49**, 299.
29 R. Dronskowski and P. E. Blöchl, *J. Phys. Chem.*, 1993, **97**, 8617.
30 V. L. Deringer, A. L. Tchougreeff and R. Dronskowski, *J. Phys. Chem. A*, 2011, **115**, 5461.
31 *Visualization for electronic and structural analysis*, http://jp-minerals.org/vesta/en/doc.html, 2016, version 3.3.9.
32 F. Ricci, W. Chen, U. Aydemir, G. J. Snyder, G.-M. Rignanese, A. Jain and G. Hautier, *An electronic transport ab initio database for inorganic materials*, 2017, submitted.
33 Y. Ogo, H. Hiramatsu, K. Nomura, H. Yanagi, T. Kamiya, M. Kimura, M. Hirano and H. Hosono, *Phys. Status Solidi A*, 2009, **206**, 2187.
34 J. B. Varley, A. Schleife, A. Janotti and C. G. Van de Walle, *Appl. Phys. Lett.*, 2013, **103**, 82118.
35 A. Togo, F. Oba, I. Tanaka and K. Tatsumi, *Phys. Rev. B: Condens. Matter Mater. Phys.*, 2006, **74**, 195128.
36 Y. Pei, W. Liu, J. Shi, Z. Chen and G. Wang, *J. Electron. Mater.*, 2016, **45**, 5967.
37 J. K. Burdett, *Chemical bonding in solids*, Oxford University Press, 1995, ch. I, p. 9.
38 W. Zhou and N. Umezawa, *Phys. Chem. Chem. Phys.*, 2015, **17**, 17816.
39 R. Hoppe and R. Nowitz, *Z. Anorg. Allg. Chem.*, 1984, **609**, 145.
40 R. M. Braun and R. Hoppe, *Angew. Chem.*, 1978, **90**, 475.
41 Y. Kang, S. H. Jeon, Y.-W. Son, Y.-S. Lee, M. Ryu, S. Lee and S. Han, *Phys. Rev. Lett.*, 2012, **108**, 196404.
42 A. Walsh, J. L. F. D. Silva and S.-H. Wei, *Chem. Mater.*, 2009, **21**, 5119.
43 M. J. Wahila, K. T. Butler, Z. W. Lebens-Higgins, C. H. Hendon, A. S. Nandur, R. E. Treharne, N. F. Quackenbush, S. Sallis, K. Mason, H. Paik, D. G. Schlom, J. C. Woicik, J. Guo, D. A. Arena, B. E. White Jr, G. W. Watson, A. Walsh and L. F. J. Piper, *Chem. Mater.*, 2016, **28**, 4706.
44 H. Mizoguchi, T. Kamiya, S. Matsuishi and H. Hosono, *Nat. Commun.*, 2011, **2**, 470.
45 A. Walsh, D. J. Payne, R. G. Egdell and G. W. Watson, *Chem. Soc. Rev.*, 2011, **40**, 4455.
46 D. Waroquiers, X. Gonze, G.-M. Rignanese, C. Welker-Nieuwoudt, F. Rosowski, M. Göbel, S. Schenk, P. Degelmann, R. André, R. Glaum and G. Hautier, *Local environments statistics in oxides from an automatic and robust detection algorithm*, 2017, submitted.